Capillary-Induced Motion of Particles Bridging Interfaces of a Free-Standing Thin Liquid Film

Abhishek Yadav,[1] E. John Hinch,[2] and Mahesh S. Tirumkudulu[1]
[1]Department of Chemical Engineering, Indian Institute of Technology Bombay, Powai, Mumbai 400076, India
[2]Department of Applied Mathematics and Theoretical Physics, University of Cambridge, Wilberforce Road, Cambridge CB3 0WA, United Kingdom

(Received 4 July 2018; revised manuscript received 20 December 2018; published 5 March 2019)

We demonstrate a new form of capillary force experienced by neutrally buoyant spherical particles adsorbed simultaneously at both interfaces of a thin liquid film of spatially varying thickness. The force is proportional to the slope of the interface and the difference between the local contact angle and the equilibrium value, and exists even when the two bounding interfaces have zero curvature. We derive the expression for the force, which when balanced against the hydrodynamic drag gives the trajectory of the particle. The measured trajectories for spherical particles of varying diameters in thin films compare well with predictions.

DOI: 10.1103/PhysRevLett.122.098001

It has been long known that colloidal particles adsorb at a liquid-liquid or liquid-gas interface and play an important role in stabilizing emulsions and foams [1–6]. More recently, there has been interest in assembling particles of varying shapes, sizes, and surface properties at interfaces in order to synthesize new materials [7,8]. These studies have mainly focused on the capillary phenomena arising at *single* interfaces from the properties of trapped particles, such as weight [9], charge [10], or shape [11], which in turn deform the surrounding interface to give rise to capillary interaction [12–14]. Interface deformation may also arise if the contact line is not in equilibrium leading to pinned contact lines and consequent particle interactions [8]. Alternatively, neutrally buoyant, uncharged, spherical particles present at curved interfaces may impose an additional deformation at the interface to satisfy the equilibrium contact angle along the three-phase contact line. This leads to a capillary force, which is proportional to the gradient of Gaussian curvature and to the mean curvature of the interface [15–17].

In contrast to the above studies, few have investigated the behavior of particles in thin films, where the particle size is comparable to the film thickness and may adsorb simultaneously at both interfaces. Such cases are especially important in understanding the role of particles in stabilizing foams [3,6,18] and emulsions [5,19,20]. The presence of ionic surfactants creates electrostatic repulsion between the interface and similarly charged particles causing the particles to move away from the thin regions of a film without adsorption at either interface [21,22]. In contrast, an oppositely charged surfactant adsorbs on the particle surface making it partially hydrophobic thereby enabling it to pierce the interface. Alternatively, high electrolyte concentration [23] or rugosities on the surface of rough particles may also facilitate interface adsorption [6,24]. Once adsorbed on both interfaces of a constant thickness aqueous film, spherical particles with contact angles greater than 90° cause the two contact lines to merge and thereby rupture the film while particles with lower contact angles stabilize the film by drawing liquid in Refs. [3,18,21,25–27]. Similarly, water-wet particles stabilize water external emulsions, while oil-wet particles stabilize oil external emulsions [19,20].

In this study, we demonstrate a new form of capillary force experienced by spherical particles that are adsorbed simultaneously at both interfaces of a liquid film with spatially varying thickness. The force arises from the difference between the local contact angle and the equilibrium contact angle, and is present even for flat interfaces, as long as the film thickness varies spatially. The capillary force pushes the particle towards a thickness where the equilibrium condition is satisfied simultaneously at both interfaces. These findings show that highly hydrophilic particles vacate the thinnest regions of an aqueous film to satisfy their equilibrium condition thereby significantly reducing the ability of particles to stabilize the film. On the contrary, particles with contact angles closer to 90° will accumulate in the thinnest regions of the film and stabilize it.

The experiments were performed using polystyrene dispersion (Sigma Aldrich), which were diluted to a very low particle volume fraction ($\sim 3 \times 10^{-4}$) using ultrapure deionized water. Experiments were performed with three different particle diameters ($2R$), namely, 3, 5, and 10 μm (CV $< 3\%$) that are typical of sizes used in emulsion stabilization [20] and defoaming applications [6,28], at a temperature of about 24 °C (± 1 °C), and a relative humidity of 35% ($\pm 2\%$). The surface tension of the dilute

suspensions was measured using the pendant drop method and was equal to 0.060 N/m. The experimental setup consisted of a rectangular frame (4 mm × 8–10 mm) of steel wires and plastic blades. A thin, free-standing film was cast in the frame with 10 μL of dispersion and placed on an inverted microscope (10×, 0.30 NA, Olympus IX71) [29]. The experiments were observed under monochromatic light so as to reveal interference fringes and therefore the time varying film thickness profile.

Circular fringes were observed at the geometric center of the film and as the film thinned due to evaporation, the fringes moved out radially from the center. When the film thickness at the center reduced to a critical value, the few particles present close to the center were pulled rapidly [$\mathcal{O}$(mm/s)] towards the center (Fig. 1, see movies in the Supplemental Material [30]). These particles then collected on an expanding circular fringe and moved radially out from the center of the film indicating that particles are attracted to a constant thickness region. During this process, particles present outside the ring remained stationary confirming the absence of bulk flow in the film. As the particle ring approached the outer particles, they were sucked radially inward into the periphery of the particle ring, while the ring itself continued to expand slowly collecting more particles (Fig. 1). No interference fringes were observed around the particles at the resolution of the microscope suggesting weak interface deformation around them. Consequently, there is negligible interaction between particles. The rapid motion of the outer particles towards a fringe followed by the slow outward motion of the particles with the radially expanding fringe indicate that the particles experience a force that pulls them to a region of fixed film thickness, which is related to their size. The hypothesis was confirmed by performing experiments with a mixture of all three particle sizes, where the aforementioned phenomenon occurred first for the largest particle size followed by 5 and by 3 μm particles eventually resulting in three expanding concentric particle rings, each coincident with a circular fringe and specific to a particle size [Fig. 2(a)].

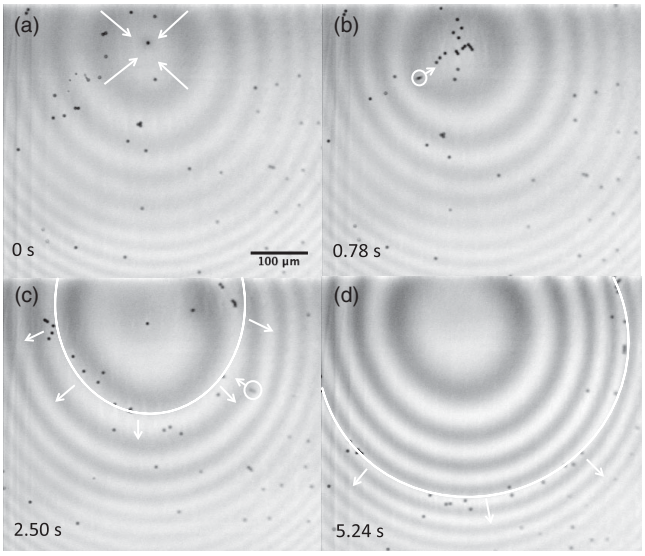

FIG. 1. Sequence of images showing the dynamics of 5 μm particles in a freely suspended, drying liquid film that eventually lead to the formation of expanding particle ring. (a) Particles close to the center of the concentric fringes are pulled towards the center, where the thickness is the lowest. The white arrows indicate the direction of particle motion. (b) A large number of particles collect at the center. The circled particle is captured at the instant when it is moving towards the center. The small time difference between the two frames suggests that the particle motion is very rapid. The particle velocities are $\mathcal{O}$(mm/s). (c) With continuing evaporation, the particles at the center collect on an expanding fringe that is highlighted by a white, curved line with arrows pointing radially outwards. Any particle present outside but close to the expanding fringe is pulled rapidly into the fringe (particle is circled). (d) The region inside the particle ring is nearly devoid of particles. See movies depicting the particle motion in the Supplemental Material [30].

The shape of the film thickness profile at any instant may be determined theoretically by solving the Young-Laplace equation for an axisymmetric film, $\kappa = (1/r)(\partial/\partial r)[r(\partial/\partial r)(h/2)] = (|\Delta P|/\gamma)$, where the small slope approximation is assumed, κ is the curvature of the interface, r is the radial coordinate, $h(r)$ is the film thickness, ΔP is the pressure difference across the liquid-gas interface and γ is the surface tension. The above equation suggests that in the absence of flow, ΔP should be independent of r implying that the curvature of the top and bottom interfaces is spatially uniform throughout the evaporation process, although the value may change with time. Integrating the above equation yields a quadratic thickness profile for the film, $h = h_0 + (\kappa/2)r^2$, where, h_0 is the film thickness at the center of the film at that instant of time. While the absolute thickness of the film is not measured in the experiments, the relative thicknesses at different radial locations are easily determined from the interference fringes [26]. The thickness difference between two consecutive bright or dark fringes is given by $\lambda/2n$ where λ is wavelength of light source and n is refractive index of fluid. For $\lambda = 561$ nm and $n = 1.33$, the measured thickness profile is plotted as a function of the square of radial distance (r^2) for an arbitrary value of h_0. As predicted, the points lie on a straight line, whose slope ($= \kappa/2$) yields the curvature of the interface [Fig. 2(b)]. The evaporation rate could be determined by noting the time required for a particular expanding fringe to reach its neighbor's position, during which time the surface drops by about half a wavelength. The rate was spatially uniform in the region of interest and was approximately 0.5 μm/s.

During the initial stages of evaporation, when the film thickness is everywhere greater than the particle size, the particles are present either in the bulk or are adsorbed at one of the two interfaces. Since the change in slope of the

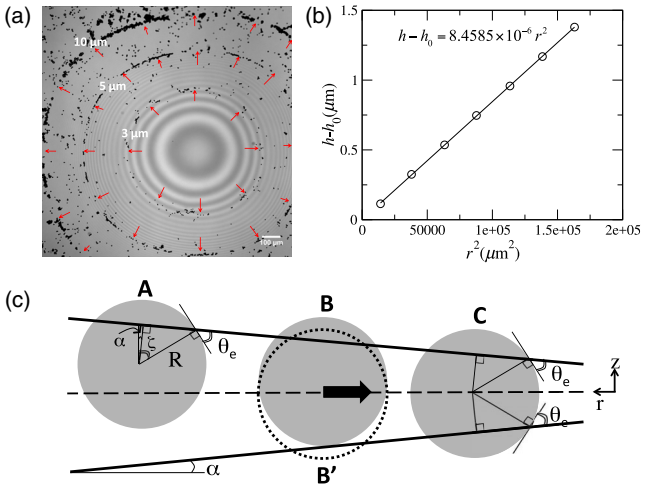

FIG. 2. (a) The images show the formation of three particle rings in a mixture of 3, 5, and 10 μm particles. The arrows indicate the direction of movement of the rings. (b) The measured thickness is fit to the predicted thickness profile, which confirms the quadratic variation with radial distance. Note that the interference image reveals the thickness profile up to an arbitrary constant with the latter corresponding to the thickness at the center of the fringe. The curvature of the interface from the fit is $\kappa = 1.68 \times 10^{-5}$ μm^{-1}. (c) The schematic shows three particles in a free-standing liquid film with spatially varying thickness. Both interfaces make an angle α with the horizontal. ζ is the distance of the adsorbed particle's center from the interface. Particle A is adsorbed at the top interface with the contact angle being equal to the equilibrium value (θ_e) while particle C is adsorbed at both interfaces with the condition of equilibrium contact angle satisfied simultaneously at both interfaces. In both cases, the particles do not experience any force. However, particle B touches the bottom interface while satisfying the equilibrium condition at the top. Since the contact angle at the bottom is different from θ_e, it will be pulled down (particle outline B') and to the right until the particle moves to the position of particle C.

interface over a particle diameter is very small ($\kappa R \ll 1$), the interface may be assumed to be flat at the length scale of the particle. Consequently, the adsorbed particle would adjust its vertical position so that the condition of equilibrium contact angle is satisfied everywhere along its three phase contact line while the interface continues to be flat at the particle length scale. With continued evaporation, the film thickness decreases everywhere causing more particles in the bulk to adsorb at one of the two interfaces. At a certain critical thickness of the film, which is related to the particle size and the equilibrium contact angle, the particles will come in simultaneous contact with both interfaces [Fig. 2(c), particle B]. At this stage, the asymmetry in the particle's vertical position with respect to the two interfaces will cause the particle to adjust its height so that the contact angle is the same at both interfaces (particle outline B') but different from the equilibrium value. As a result, the particle will experience a transverse force in the direction where the contact angle at both interfaces will eventually be equal to the equilibrium value.

The mathematical expression for the transverse force experienced by the particles may be derived from energy considerations [10]. For a particle adsorbed at a single interface, the total surface energy for a flat interface is given by

$$E_{\text{single}}(\zeta) = \gamma_{\text{SA}}(2\pi R^2 - 2\pi R\zeta) + \gamma_{\text{SL}}(2\pi R^2 + 2\pi R\zeta) - \gamma_{\text{LA}}\pi(R^2 - \zeta^2), \quad (1)$$

where γ_{SA}, γ_{SL}, and γ_{LA} are the solid-air, solid-liquid, and liquid-air interfacial tensions, respectively. Here, ζ is the distance of the particle center from the interface [Fig. 2(c)]. The first two terms on the right side correspond to the interfacial energy of the solid-air and solid-liquid interfaces while the last term accounts for the missing liquid-air interface. Minimizing the total energy with respect to ζ gives the equilibrium position of the particle at a single interface, $\zeta_e = R[(\gamma_{\text{SA}} - \gamma_{\text{SL}})/\gamma_{\text{LA}}] \equiv R\cos\theta_e$, where θ_e is the equilibrium contact angle. In this case, the particle will experience a force perpendicular to the interface if it is displaced away from ζ_e, with the force being proportional to the distance from the equilibrium position but it will not experience any transverse force. However, when the particle is adsorbed simultaneously at both interfaces of a freely suspended film whose thickness varies spatially, the particle will experience a transverse force in the direction of decreasing energy,

$$F = 2 \times -\frac{dE_{\text{single}}}{dr} = -4\pi\gamma_{\text{LA}}(\zeta - \zeta_e)\frac{d\zeta}{dr}. \quad (2)$$

This is because the contact angle is different from the equilibrium value and so the particle will continue to move in the transverse direction until the condition of equilibrium contact angle is satisfied simultaneously at both interfaces or towards the lowest energy position, whichever is accessible. As a simplification, the model assumes the interface around the particle to be flat and the particle to be located symmetrically with respect to the midplane of the film during its motion. The latter contributes a factor of 2 in the above expression. An alternate expression for force may be derived by assuming the contact angle to be always equal to the equilibrium value but it results in a curved interface around the particle, which was not observed at the resolution of the microscope (see Supplemental Material [30]).

The distance ζ is related to the local thickness and the local slope of the interface (α), $\zeta = (h/2)\cos\alpha$, so that the net force is now proportional to the slope of the interface, $F = -\pi\gamma_{\text{LA}}(h - h_e)(dh/dr)\cos^2\alpha$. Since the slopes are very small in the experiments ($\kappa r \ll 1$), $\cos^2\alpha \approx 1$. The moving particle is retarded by viscous drag, whose expression may be approximated by $F_{\text{drag}} = \pi\mu h V f_d$, where μ is

the liquid viscosity and V is the speed of the particle. The approximation is based on the drag experienced by a cylindrical particle moving in a thin sheet of viscous liquid that is embedded in fluid of a much lower viscosity [33]. The numerical constant f_d is a fitting parameter and reflects the uncertainties in approximating a partially immersed sphere to a cylinder.

The particle dynamics will be governed by force balance, which in dimensionless form is given by

$$\frac{4}{3}\frac{\bar{\kappa}^2}{f_d^2 \mathrm{Oh}^2}\frac{d^2\bar{r}}{d\bar{t}^2} = -\frac{1}{2}\bar{r}(\bar{r}^2 - \bar{r}_e^2) - \left(\frac{\bar{\kappa}}{2}\bar{r}^2 + \bar{h}_0\right)\frac{d\bar{r}}{d\bar{t}},$$

where the characteristic length scale is chosen to be the particle radius, the characteristic timescale as $\mu R f_d/\gamma_{\mathrm{LA}}(\kappa R)^2$, and the Ohnesorge number is given by, $\mathrm{Oh} \equiv \mu/\sqrt{\rho R \gamma_{\mathrm{LA}}}$, with ρ being the density of the particle. Here, $\bar{r}_e$ is the position where the equilibrium condition is satisfied simultaneously at both interfaces. In experiments, the rapid motion of the particles occurs towards the center of the film ($\bar{r} > \bar{r}_e$), which is in line with the negative sign of the second term. Since $\bar{\kappa} \sim \mathcal{O}(10^{-5})$ and $\mathrm{Oh} \sim \mathcal{O}(10)$ in all experiments, the inertial term may be neglected thereby enabling an analytical expression for the trajectory of the particle,

$$\bar{t} = \frac{2\bar{h}_0}{\bar{r}_e^2}\ln\left(\frac{\bar{r}}{\bar{r}_i}\right) - \frac{1}{2}\left(\bar{\kappa} + \frac{2\bar{h}_0}{\bar{r}_e^2}\right)\ln\left(\frac{\bar{r}^2 - \bar{r}_e^2}{\bar{r}_i^2 - \bar{r}_e^2}\right). \quad (3)$$

The time evolution of the particle position requires the knowledge of the film thickness $\bar{h}_i$ at the initial position $\bar{r}_i$. This is obtained by noting that the particle first comes in simultaneous contact with both interfaces at $\bar{r}_i$ [particle B in Fig. 2(c)] before moving towards the equilibrium location $\bar{r}_e(< \bar{r}_i)$. At $\bar{r}_e$, however, the equilibrium contact angle is satisfied at both interfaces. These geometric constraints together with the equation for film thickness give two equations,

$$\frac{1+\cos\theta_e}{\cos\alpha_i} = \left(\frac{\bar{\kappa}}{2}\bar{r}_i^2 + \bar{h}_0\right), \qquad \frac{2\cos\theta_e}{\cos\alpha_e} = \left(\frac{\bar{\kappa}}{2}\bar{r}_e^2 + \bar{h}_0\right), \quad (4)$$

where, $\cos\alpha_{i,e} \approx 1$. The two Eqs. (4) are solved simultaneously to obtain $\cos\theta_e$ and h_0 and, subsequently, h_i and h_e.

Before comparing the predictions with measurements, it is instructive to obtain an approximate form of Eq. (3). Since $\bar{\kappa} \ll 1$ in all experiments, the slope may be assumed to be constant over the trajectory of the particle. Further, if h is replaced with $2R$ in the expression for drag, then the trajectory of the particle follows a decreasing exponential function in time, $(\bar{r}-\bar{r}_e)/(\bar{r}_i-\bar{r}_e) \approx \exp[-(2\gamma_{LA}\sin^2\alpha/\mu R f_d)t]$. Consequently, the velocity of the particle is proportional to the square of the slope of the interface. Further, the timescale of motion is small, $\mu R f_d/2\gamma_{\mathrm{LA}}\sin^2\alpha \sim \mathcal{O}(0.1s)$, which confirms the rapid motion observed in experiments. The observed motion is distinct from those due to capillary interactions between particles where the force varies with some inverse power of the distance between particles [8]. In such cases, the particles start off slowly and accelerate towards a neighbor [11].

Equation (3) is solved to compare the predicted trajectory with measurements for particles during their rapid motion in the radially inward direction towards an expanding fringe (Fig. 3). The error bars along the dimensionless time axis correspond to half the time difference between frames while that along the dimensionless distance axis corresponds to the length of the image pixel. Overall, there is good match for all three particle sizes as the model is able to capture the salient features of the trajectory. As the particle slows down while approaching its equilibrium thickness, the corresponding expanding fringe captures the particle. This leads to some discrepancy towards the end of the particle's trajectory. The larger than expected value of f_d suggests that the capillary force is somewhat

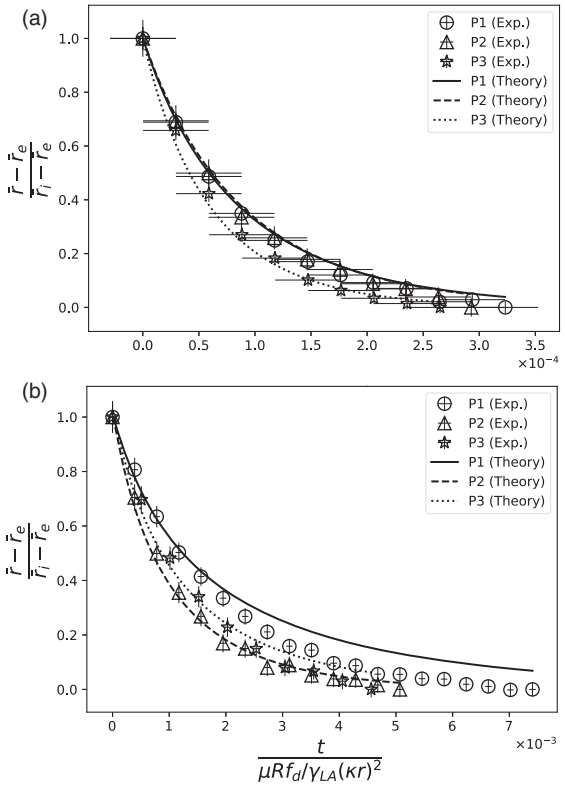

FIG. 3. The three plots compare the prediction (3) with measurements for three trajectories, each for (a) 3, and (b) 10 μm particles. The corresponding (average $\pm$ SD) values of equilibrium contact angle for the three particles obtained from Eq. (4) were $33.2° \pm 4.6°$ and $24.0° \pm 0.7°$, while f_d was equal to 15 and 5, respectively. See Supplemental Material [30] for data on 5 μm particles and contact angles [30].

lower than that predicted by the model. One possible reason could be the assumption of a constant angle along the contact line during the particle's motion although the contact angle may vary between a receding and an ascending contact angle that will reduce the capillary force on the particle.

Notwithstanding the aforementioned complexities, the new motion we demonstrate is all about the size of particles and the thickness of the film. What is interesting is that the small variations between the different particles seem not to matter, in that all the 3, the 5 and the 10 μm particles collect in the same or adjacent fringe. Hence, what we observe is quite a robust phenomenon. Finally, the addition of anionic surfactant eliminates the rapid, radially inward motion and reproduces the previous observation of interface wrapping and slow, radially outward motion towards thicker regions [22] (See Supplemental Material [30]).

One of the most intriguing aspects of the phenomenon is that the transverse capillary force acts even for flat interfaces in varying thickness films. Our results highlight the importance of accounting for variable thickness in films stabilized by particles as they support the longstanding observation that spherical particles with $75° < \theta_e < 90°$ yield the most stable aqueous foams [6,34], and that particles with θ_e slightly greater than 90° stabilize oil-in-water emulsions while those with slightly lower than 90° stabilize water-in-oil emulsions [19,20]. In all these cases, the bridging particles experience a capillary force towards the thinnest regions thereby preventing early film rupture, even at low particle volume fractions [35–37].

A. Y. thanks IIT Bombay for financial support. M. S. T. acknowledges financial support from Trinity College, Cambridge University and EJH from GIAN scheme of Ministry of Human Resource Development, Government of India that enabled the collaboration. The project was funded in part by Department of Science and Technology, India.

[1] S. U. Pickering, J. Chem. Soc. **91**, 2001 (1907).
[2] P. Finkle, H. D. Draper, and J. H. Hildebrand, J. Am. Chem. Soc. **45**, 2780 (1923).
[3] R. Aveyard, B. P. Binks, P. D. I. Fletcher, T. G. Peck, and C. E. Rutherford, Adv. Colloid Interface Sci. **48**, 93 (1994).
[4] R. J. Pugh, Adv. Colloid Interface Sci. **64**, 67 (1996).
[5] B. P. Binks, Curr. Opin. Colloid Interface Sci. **7**, 21 (2002).
[6] P. R. Garrett, *The Science of Defoaming* (CRC Press, Boca-Raton, 2014).
[7] B. P. Binks, Langmuir **33**, 6947 (2017).
[8] I. B. Liu, N. Sharifi-Mood, and K. J. Stebe, Annu. Rev. Condens. Matter Phys. **9**, 283 (2018).
[9] M. M. Nicolson, Proc. Cambridge Philos. Soc. **45**, 288 (1949).
[10] P. Pieranski, Phys. Rev. Lett. **45**, 569 (1980).
[11] J. C. Loudet, A. M. Alsayed, J. Zhang, and A. G. Yodh, Phys. Rev. Lett. **94**, 018301 (2005).
[12] D. Y. C. Chan, J. D. Henry, and L. R. White, J. Colloid Interface Sci. **79**, 410 (1981).
[13] P. A. Kralchevsky and K. Nagayama, Langmuir **10**, 23 (1994).
[14] *Colloidal Particles at Liquid Interfaces*, edited by B. P. Binks and T. S. Horozov (Cambridge University Press, Cambridge, England, 2006).
[15] A. Wurger, Phys. Rev. E **74**, 041402 (2006).
[16] C. Blanc, D. Fedorenko, M. Gross, M. In, M. Abkarian, M. A. Gharbi, J.-B. Fournier, P. Galatola, and M. Nobili, Phys. Rev. Lett. **111**, 058302 (2013).
[17] D. Ershov, J. Sprakel, J. Appel, M. A. Cohen Stuart, and J. van der Gucht, Proc. Natl. Acad. Sci. U.S.A. **110**, 9220 (2013).
[18] P. R. Garrett, J. Colloid Interface Sci. **69**, 107 (1979).
[19] J. H. Schulman and J. Leja, Trans. Faraday Soc. **50**, 598 (1954).
[20] D. E. Tambe and M. M. Sharma, Adv. Colloid Interface Sci. **52**, 1 (1994).
[21] K. P. Velikov, F. Durst, and O. D. Velev, Langmuir **14**, 1148 (1998).
[22] J. Sur and H. K. Pak, Phys. Rev. Lett. **86**, 4326 (2001).
[23] D. M. Kaz, R. McGorty, M. Mani, M. P. Brenner, and V. N. Manoharan, Nat. Mater. **11**, 138 (2012).
[24] M. Zanini, C. Marschelke, S. E. Anachkov, E. Marini, A. Synytska, and L. Isa, Nat. Commun. **8**, 15701 (2017).
[25] A. Dippenaar, Int. J. Miner. Process. **9**, 1 (1982).
[26] T. S. Horozov, D. A. Braz, P. D. I. Fletcher, B. P. Binks, and J. H. Clint, Langmuir **24**, 1678 (2008).
[27] A. Yadav and M. S. Tirumkudulu, Soft Matter **13**, 4520 (2017).
[28] N. D. Denkov and K. G. Marinova, in *Colloidal Particles at Liquid Interfaces*, edited by B. P. Binks and T. S. Horozov (Cambridge University Press, Cambridge, England, 2006), pp. 383–444.
[29] R. Sengupta and M. S. Tirumkudulu, Soft Matter **12**, 3149 (2016).
[30] See Supplemental Material at http://link.aps.org/supplemental/10.1103/PhysRevLett.122.098001 for additional details. It is divided into six sections: I. Derivation of capillary force from equilibrium contact angle, II. experiments: Materials and methods, III. experiments with surfactant, IV. trajectory data for 5 μm particles, V. contact angle distribution, and VI. movies. It also includes Refs. [31] and [32].
[31] A. Maestro, E. Guzmanb, F. Ortega, and R. G. Rubio, Curr. Opin. Colloid Interface Sci. **19**, 355 (2014).
[32] C. Snoeyink, S. Barman, and G. F. Christopher, Langmuir **31**, 891 (2015).
[33] P. G. Saffman, J. Fluid Mech. **73**, 593 (1976).
[34] R. Aveyard, B. P. Binks, P. D. I. Fletcher, and C. E. Rutherford, J. Dispersion Sci. Technol. **15**, 251 (1994).
[35] E. Vignati, R. Piazza, and T. P. Lockhart, Langmuir **19**, 6650 (2003).
[36] E. J. Stanick, M. Kouhkan, and G. G. Fuller, Langmuir **20**, 90 (2004).
[37] R. J. Lopetinsky, J. H. Masliyah, and Z. Xu, in *Colloidal Particles at Liquid Interfaces*, edited by B. P. Binks and T. S. Horozov (Cambridge University Press, Cambridge, England, 2006), pp. 186–224.